1 **Title**

2 Chronic innate immune impairment and ZIKV persistence in the gastrointestinal tract during SIV

3 infection in pigtail macaques

4

5 **Short Title**

6 Innate immune impairment and ZIKV persistence in the gut during SIV infection

7

8 **Authors**

9 Jennifer Tisoncik-Go[1,2,3], Thomas B. Lewis[1, 4], Leanne S. Whitmore[2], Kathleen Voss[1,2], Skyler

10 Niemeyer[4], Jin Dai[2], Paul Kim[4], Kai Hubbell[4], Naoto Iwayama[1], Chul Ahrens[1], Solomon

11 Wangari[1], Robert Murnane[1], Paul T. Edlefsen[5], Kathryn A. Guerriero[1], Michael Gale Jr[1, 2, 3, 6],

12 Deborah H. Fuller[1, 4], Megan A. O'Connor[1, 4]

13

14 **Affiliations**

15 [1]Washington National Primate Research Center, University of Washington (Seattle,

16 Washington)

17 [2]Department of Immunology, University of Washington (Seattle, Washington)

18 [3]Center for Innate Immunity and Immune Disease (CIIID), University of Washington (Seattle,

19 Washington)

20 [4]Department of Microbiology, University of Washington (Seattle, Washington)

21 [5]Fred Hutchinson Cancer Center (Seattle, Washington)

22 [6]Department of Global Health, University of Washington (Seattle, Washington)

23

24

25

26

Abstract

Mosquito borne flaviviruses, including dengue (DENV) and Zika (ZIKV) viruses, have caused global epidemics in areas with high HIV prevalence due to the expanded geographic range of arthropod vectors. Despite the occurrence of large flavivirus outbreaks in countries with high HIV prevalence, there is little knowledge regarding the effects of flavivirus infection in people living with HIV (PLWH). Here, we use a pigtail macaque model of HIV/AIDS to investigate the impact of simian immunodeficiency virus (SIV)-induced immunosuppression on ZIKV replication and pathogenesis. Early acute SIV infection induced expansion of peripheral ZIKV cellular targets and increased innate immune activation and peripheral blood mononuclear cells (PBMC) from SIV infected macaques were less permissive to ZIKV infection *in vitro*. In SIV-ZIKV co-infected animals, we found increased persistence of ZIKV in the periphery and tissues corresponding to alterations in innate cellular (monocytes, neutrophils) recruitment to the blood and tissues, decreased anti-ZIKV immunity, and chronic peripheral inflammatory and innate immune gene expression. Collectively, these findings suggest that untreated SIV infection may impair cellular innate responses and create an environment of chronic immune activation that promotes prolonged ZIKV viremia and persistence in the gastrointestinal tract. These results suggest that PLWH or other immunocompromised individuals could be at a higher risk for chronic ZIKV replication, which in turn could increase the timeframe of ZIKV transmission. Thus, PLWH are important populations to target during the deployment of vaccine and treatment strategies against ZIKV.

Author Summary

Flaviviruses, including Zika virus (ZIKV), cause global epidemics in areas with high HIV prevalence. Yet questions remain as to whether ZIKV disease is altered during an immunocompromised state and the potential immune mechanisms contributing to enhanced disease. This is essential to our understanding of ZIKV disease in people living with HIV (PLWH).

53   Here, we use a non-human primate (NHP) model of HIV/AIDS to investigate the impact of immune

54   suppression on ZIKV replication and pathogenesis. The use of the NHP model was critical for the

55   assessment of longitudinal specimens across tissues that are active sites of flavivirus replication

56   and host immune responses. This study broadly demonstrates that ZIKV pathogenesis is altered

57   and more persistent in states of immunosuppression. Collectively, this study suggests that in

58   PLWH and immunocompromised individuals, other arboviruses, including dengue and West Nile

59   viruses, could similarly alter pathogenesis and/or viral peristance in tissues. Furthermore, this

60   study highlights the need to prioritize immunocompromised individuals in the design and rollout

61   of vaccines against arboviral diseases.

62

Introduction

Flaviviruses, including dengue (DENV), West Nile (WNV), yellow fever (YFV), and Zika (ZIKV) viruses, are single-stranded RNA viruses that are transmitted to people through the bite of an infected mosquito and have caused global epidemics in recent years. Flavivirus infection commonly causes mild clinical manifestations; however, more severe hemorrhagic or encephalitic disease can occur and the mechanisms underlying severe disease are not fully understood. Furthermore, vulnerable populations including children, pregnant women, and immunocompromised individuals, including people living with HIV (PLWH) may be at a higher risk for more severe flavivirus disease. Currently, highly effective vaccines against DENV, WNV, and ZIKV do not exist. While the live-attenuated YFV vaccine 17D is available, it is contraindicated in infants and in immunosuppressed individuals and is relatively contraindicated in the elderly, pregnant women, and PLWH due to poor immunogenicity or severe adverse reactions[1-4]. Therefore, there is a need to better understand flavivirus pathogenesis in at risk populations.

ZIKV transmission is primarily via mosquito bite; however, transmission also occurs through sexual intercourse and from mother to fetus[5-7]. ZIKV infection usually results in mild and self-limiting symptoms, but it is also associated with the neurological disorder Guillain-Barré syndrome (GBS) in adults and congenital Zika syndrome (CZS) during *in utero* exposure[8, 9]. CZS is characterized by severe defects in cranial morphology, ocular abnormalities, muscle contractures and neurological impairments[10]. ZIKV-exposed children have impaired neurodevelopment, but the long-term effects in ZIKV exposed infants remains an active area of investigation as children exposed during the 2015-2016 outbreak in the Americas are now school aged[11-13]. Nonhuman (NHP) models of ZIKV infection mimic the many routes of ZIKV infection, mild human disease, and recapitulate vertical transmission and severe aspects of CZS[14-18]. In NHP models of ZIKV vertical transmission, fetal loss was reported in 26% of ZIKV exposed animals and suggests fetal loss in asymptomatic ZIKV infected women may go underreported[16]. Moreover, altered myelination in normocephalic fetuses following maternal-to-fetal ZIKV

4

89   transmission argues ZIKV infection *in utero* can impact pre- and post-natal neurologic

90   development(19). Therefore, the NHP is an ideal model for understanding the mechanisms of

91   human ZIKV infection and for testing ZIKV vaccines.

92   Innate and adaptive immune responses are important for ZIKV viral clearance and

93   protection against re-infection(20, 21). We and others have found that circulating monocytes and

94   dendritic cells are the major cellular blood targets of ZIKV infection in humans and NHP and can

95   contribute to disease pathogenesis by the production of inflammatory mediators(22-24). Yet,

96   these cells are also potently activated during ZIKV infection and contribute to the antiviral type I

97   interferon response(25). Blood monocyte frequencies increase during HIV infection and although

98   antiretroviral therapy (ART) reduces total monocyte frequencies in PLWH, inflammatory

99   monocytes remain elevated(26). We therefore hypothesized that altered innate immune

100 responses during HIV infection could promote susceptibility to ZIKV infection and alter ZIKV

101 pathogenesis. Here, using the pigtail macaque model of HIV/AIDS, we evaluated the impact of

102 simian immunodeficiency virus (SIV) infection on the susceptibility of peripheral blood

103 mononuclear cells (PBMC) to ZIKV infection, ZIKV persistence and host immunity.

104

105 **Results**

106 ***In vitro ZIKV replication is impaired in PBMC from NHP acutely infected with SIV.***

107 Pigtail macaques (n=7) were infected with SIVmac239M and blood was collected prior to and at

108 2 and 6 weeks post-SIV infection. Both post-infection timepoints are associated with significant

109 declines in peripheral CD4 counts and correspond with SIV peak and viral setpoint, respectively

110 (**Supplemental Figure 1A and C**). To evaluate whether SIV infection alters the permissivity of

111 peripheral blood mononuclear cells (PBMC) to Zika virus (ZIKV) infection, we isolated fresh PBMC

112 from naïve (Pre-SIV) and SIV+ (Weeks 2 and 6) PTM (n=4) and inoculated cells with ZIKV Brazil

113 2015 (MOI of 2) *ex vivo*. At 4, 24 and 48 hours post-ZIKV infection (hpi), cells and culture

114 supernatants were collected to measure ZIKV RNA and viral titer. Pre-SIV PBMC were permissive

115   to ZIKV infection, as measured by qRT-PCR and plaque assay, with peak viral replication at 24

116   hpi (**Figure 1A-B, Supplemental Figure 2**). ZIKV RNA levels in Week 2 SIV+ PBMC were

117   significantly decreased at 24 and 48 hpi compared to pre-SIV PBMC, while Week 6 SIV+ PBMC

118   had similar ZIKV RNA levels to that in pre-SIV PBMC (**Figure 1A**). The kinetics of ZIKV replication

119   in pre-SIV PBMC were similar in PBMC derived from SIV$^+$ PTM; however, significantly lower levels

120   of infectious virus were observed at 24 and 48 hpi in Week 6 SIV+ PBMC (**Figure 1B,**

121   **Supplemental Figure 2**). Supernatants from ZIKV-infected PBMC cultures were subjected to

122   multiplex immunoassay to measure cytokine and chemokine concentration changes at 4, 24, and

123   48 hpi. All cultures accumulated the pro-inflammatory cytokines MCP-1 and VEGF-A during the

124   48 hr post-infection period; however, there was only a trend for an increase of IL-5 (p = 0.061) in

125   Week 2 SIV-infected cultures relative to pre-SIV at 24 hr (**Supplemental Figure 3**). These data

126   suggest that cells from acutely SIV-infected animals are less permissive to ZIKV infection.

127

128   ***Expansion of ZIKV cellular targets in the blood during acute SIV infection.***

129   Monocyte frequencies increase in the blood during HIV and SIV infection and are the primary

130   targets of ZIKV infection(22-24, 26). Since ZIKV replication was reduced in PBMC derived from

131   SIV-infected animals, we wanted to determine whether this may be due to decreased ZIKV

132   cellular targets. To test this, we evaluated innate cells in fresh blood from SIV+ and SIV- PTM by

133   flow cytometry. During acute SIV infection, there was a median 2.7-fold increase in the frequency

134   of CD16+ monocytes and a median 9.0-fold increase in the frequency of dendritic cells (DCs) at

135   Week 2, with levels returning to pre-infection levels at Week 6 (**Figure 1C**). AXL, a TAM receptor

136   tyrosine kinase, expressed on monocytes, macrophages, and DCs mediates ZIKV entry into

137   human glial, endothelial, and fetal endothelial cells(34-37). *In vitro* HIV infection of monocyte-

138   derived macrophages causes a 1.5-fold increase in AXL gene expression(38), but it remains

139   unknown if this also occurs *in vivo*. *Ex vivo* AXL expression on CD16+ monocytes and DCs was

140   unchanged at Weeks 2 or 6 post SIV-infection (**Supplemental Figure 4**). Thus, PBMC from SIV-

141   infected PTM have similar/greater levels of ZIKV cellular targets in comparison to naïve PTM and

142   these cells express similar levels of surface AXL, but are less vulnerable to ZIKV infection *ex vivo*.

143   We next hypothesized that anti-viral responses induced early within SIV infection could

144   influence ZIKV permissibility. To test this, we used a targeted custom-built NanoString nCounter

145   gene expression assay to investigate a panel of immune-related genes (84 genes) in PBMC

146   collected at pre-SIV and at Weeks 2 and 6 post-SIV infection. Differential gene expression

147   analysis using a t-test was performed for each time-point post-SIV infection relative to pre-SIV

148   PBMC identified several innate immune and interferon stimulated genes (ISGs) that were

149   significantly upregulated (**Figure 1D, Supplemental Table 4**). With SIV infection, several genes

150   related to innate immunity were upregulated in expression compared to pre-SIV PBMC. Notably,

151   *IFIT1*, *MX2*, and *OAS1* ISGs were increased in expression at both Weeks 2 and 6 post-SIV.

152   *ISG20* and *ISG15* were significantly upregulated in expression at Week 6, while *CXCL8* and *CCL2*

153   encoding monocyte chemoattractant protein were significantly upregulated at Week 2 post-SIV.

154   Retinoic acid-inducible gene-I (RIG-I) signaling activates the expression of these antiviral genes

155   that, in turn, are known to restrict ZIKV replication(39, 40). These data indicate that despite the

156   presence and expansion of ZIKV cellular targets during acute SIV infection, increased innate

157   immune responses in PBMC could render monocytes refractory to ZIKV infection.

158

159   ***ZIKV co-infection does not significantly impact peripheral SIV disease progression***

160   SIV-infected PTM were co-infected with ZIKV at 63 days (9 weeks) post-SIV infection

161   (SIV+ZIKV+) and compared to SIV-naïve PTM infected with ZIKV (SIV-ZIKV+) (**Figure 2A**). This

162   timepoint post-SIV was selected as an early chronic phase of SIV infection and corresponds with

163   the establishment of viral setpoint (median SIV viremia 5.41 (1.63-6.18) $\log_{10}$ copies/mL of

164   plasma) and evidence of immunosuppression including lowered, yet stable peripheral CD4 counts

165   (median 399 (333-901) cells/μL of blood) and decreased frequencies of CD4 T-cells in the gut

166   mucosa relative to SIV-naïve controls (**Supplemental Figure 1C-E, Supplemental Table 1**).

7

167   Blood, peripheral lymph nodes (PLN), cerebrospinal fluid (CSF), and rectal samples (biopsy,

168   cytobrush) were longitudinally collected according to **Figure 2A** for 4 weeks until the time of

169   necropsy. In the SIV+ZIKV+ cohort, SIV viremia and peripheral CD4 counts remained stable post-

170   ZIKV coinfection and there was no evidence of enhanced gut barrier dysfunction (**Supplemental**

171   **Figure 1C-E, 5A**). The most notable histologic findings were in Z16197, who had the syndrome

172   proliferative-occlusive pulmonary arteriopathy with thrombosis and infarction, which is a retroviral-

173   strain-associated disease that was likely secondary to the SIV infection **(Supplemental Table 2)**.

174   Overall, these findings suggest that acute ZIKV co-infection does not have a significant effect on

175   SIV viral replication or disease progression.

176

177   ***SIV infection promotes delayed ZIKV viremia and increases ZIKV persistence in the gut***

178   ***mucosa***

179   To assess the impact of the early chronic phase of SIV infection on ZIKV pathogenesis and tissue

180   tropism, ZIKV burden was evaluated in longitudinal specimens and in tissues at necropsy by qRT-

181   PCR. ZIKV RNA was not detected in one animal in the SIV+ZIKV+ cohort (Z14109) in any

182   longitudinal sample tested nor in any necropsy tissue (**Supplemental Table 7-8**); therefore, there

183   was no evidence of productive ZIKV infection, and the animal was excluded from all subsequent

184   post-ZIKV analysis. In the SIV-ZIKV+ cohort, plasma viremia peaked 2-4 days post infection (dpi)

185   (median 3 dpi) and ZIKV was cleared in the plasma in most animals (6/7) by 7 dpi (**Figure 2B**),

186   and the mean viral kinetics in this cohort was consistent with our previous findings in ZIKV-infected

187   PTM(24). In contrast, in SIV+ZIKV+ PTM, peak ZIKV viremia was variable (1-10 dpi; median 4

188   dpi) and virus was still present in most animals (4/7) by 7 dpi (**Figure 2B**). Accordingly, median

189   plasma viral loads at 2 and 3 dpi trended to be higher or significantly higher (2 dpi, $p = 0.108$; 3

190   dpi $p = 0.050$) in the naïve animals compared to SIV+ZIKV+ PTM and, but instead trended higher

191   ($p=0.054$) in SIV+ZIKV+ PTM at 7 dpi (**Supplemental Figure 6A**). Together, these data indicate

192   that initial ZIKV viremia and clearance in the periphery are delayed in SIV-infected macaques.

193   We next examined ZIKV burden in longitudinal PLN, rectal tissue biopsies, and CSF

194   collected at days 4, 7 and 21 post-ZIKV challenge, as these are known sites of ZIKV tropism(14,

195   24). In PLN, ZIKV RNA was detected in most animals (SIV- 5/7; SIV+ 4/6) and in a proportion of

196   animals (SIV- 2/7; SIV+ 2/6) at 7 and 21 dpi, respectively (**Figure 2B**). In rectal biopsy tissue,

197   ZIKV RNA was detected in 4/7 of SIV- and 2/6 of SIV+ animals at 7 dpi, and at the time of necropsy

198   (24-18 DPI) was detected in 1/7 of SIV- and 3/6 of SIV+ animals at necropsy (**Figure 2B,**

199   **Supplemental Figure 6**), providing evidence for ZIKV persistence in the rectum during SIV

200   infection. In rectal cytobrushes, ZIKV RNA was predominantly detected in SIV- animals at 7 dpi

201   (4/7 PTM) and was sporadically, but more consistently detected in SIV+ animals at 10 dpi (4/6

202   PTM) and the total viral burden trended ($p = 0.171$) to be higher during SIV+ZIKV+ co-infection

203   (**Figure 2B, Supplemental Figure 6**). ZIKV RNA was not detected in CSF of any animal at any

204   timepoint throughout the study (**Supplemental Table 7**). Overall, these data suggest that ZIKV

205   infectivity of the gut mucosa may persist during untreated SIV infection.

206   To evaluate the impact of SIV infection on ZIKV tropism and persistence in tissues, we

207   measured ZIKV viral burden in lymphoid, gut mucosal, and neuronal tissues at necropsy (24-28

208   dpi). In both cohorts, ZIKV RNA was detected in both lymphoid and gastrointestinal tissues, but

209   not in brain tissue (brainstem, hippocampus, frontal lobe, parietal lobe, and occipital lobe), which

210   further corroborates findings in the CSF suggesting that ZIKV was not neurotropic in the animals

211   (**Figure 2C, Supplemental Table 8**). The total number of ZIKV+ tissues at necropsy trended

212   higher in SIV+ZIKV+ animals ($p = 0.108$) compared to SIV-ZIKV+ animals (**Supplemental Figure**

213   **7A**). Upon further examination, ZIKV RNA was detected in at least one lymphoid tissue in most

214   animals from each cohort (5/6 SIV+ZIKV+; 5/7 SIV-ZIKV+) at necropsy and the median number

215   of positive tissues at necropsy was 4.5 for SIV+ and 1.0 for SIV- PTM (**Figure 2C, Supplemental**

216   **Figure 7**). There was no significant difference in the number of positive lymphoid tissues or in the

217   individual or total ZIKV viral burden within lymphoid tissues (**Supplemental Figure 7**). At

218   necropsy, ZIKV RNA was detected in at least one gut associated tissue in a majority (5/6) of SIV+

9

219   PTM but only in 2/7 SIV- PTM (**Figure 2C**). In accordance, the median number of ZIKV+

220   gastrointestinal tissues trended (p = 0.057) to being higher in SIV-infected PTM (**Supplemental**

221   **Figure 7**) and there trended to be a greater total (p = 0.125) gut ZIKV viral burden during SIV co-

222   infection (**Supplemental Figure 7**). Collectively, these data suggest that ZIKV distribution and

223   viral burden is similar in the lymphoid tissues, but that SIV infection could contribute to greater

224   ZIKV persistence in gut mucosal tissues.

225

226   ***Delayed and dampened expansion of ZIKV cellular targets in blood corresponds with the***

227   ***recruitment of cellular targets to tissues during SIV-ZIKV coinfection.***

228   As there was evidence for altered ZIKV pathogenesis in SIV-infected animals, we next wanted to

229   evaluate whether this was associated with changes to ZIKV cellular targets or the immune

230   response. Humoral responses are important for the control of ZIKV infection(41) and we

231   measured anti-ZIKV envelope IgG responses in longitudinal plasma samples. SIV-ZIKV+ animals

232   generated robust binding IgG antibodies that were detected at 7 dpi and peaked at 14 dpi. In

233   contrast, anti-ZIKV envelope IgG responses were lower overall in SIV+ZIKV+ animals (AUC, p =

234   0.014) (**Figure 3A**). Despite the difference in anti-ZIKV IgG between the two cohorts, there was

235   a similar level of neutralizing antibodies (NAb) generated against ZIKV at necropsy (7/7 SIV-

236   ZIKV+, 6/7 SIV+ZIKV+), with no significant difference in the overall NAb level between groups

237   (**Figure 3B**).

238   Consistent with our previous findings(24), there is rapid and robust expansion of

239   inflammatory CD16+ (non-classical and intermediate) and CD16- (classical) monocytes in the

240   blood in the first few days after ZIKV infection (median peak 2 dpi), which corresponds to peak

241   ZIKV viremia (**Figure 4A, Supplemental Figure 8**). In contrast, the expansion of CD16+ and

242   CD16- monocytes was severely dampened and delayed during SIV infection (median peak 8.5

243   days) (**Figure 4A, Supplemental Figure 8**) and corresponded with the delayed peak ZIKV

244   viremia observed in these animals (**Figure 2B**). Cellular analysis in the tissues revealed that

10

245   CD16- monocytes/macrophages were robustly and significantly recruited to the rectum and PLN

246   in SIV- negative animals, whereas in contrast CD16+ monocytes/macrophages were recruited to

247   the tissues during SIV+ZIKV+ co-infection (**Figure 4A, Supplemental Figure 8**). Additionally,

248   AXL expression was not significantly changed on ZIKV cellular targets in whole blood, rectum and

249   PLN in either group post-ZIKV infection (**Supplemental Figure 9**). These findings suggest that

250   increased recruitment of inflammatory monocytes and macrophages to lymphoid and

251   gastrointestinal tissues during SIV infection, which are also cellular targets of Zika virus infection,

252   may contribute to ZIKV viral persistence at these sites.

253   Neutrophils are important for ZIKV dissemination and pathogenesis(24, 42, 43). Blood

254   neutrophils declined during SIV+ZIKV+ co-infection starting at 1 dpi and were significantly lower

255   in frequency in comparison to SIV-ZIKV+ animals through 21 dpi (**Figure 4B**). The frequencies of

256   neutrophils in the tissues were also lower in SIV+ZIKV+ compared to SIV-ZIKV+ animals in the

257   rectum at 21 dpi, with no differences in neutrophil frequencies observed within the PLN

258   (**Supplemental Figure 10**). To assess neutrophil function, we evaluated plasma concentrations

259   of myeloperoxidase (MPO), a neutrophil granule and marker of inflammation, during the first 4

260   days of ZIKV infection. Interestingly, prior to ZIKV infection, elevated levels of MPO were detected

261   in 5/6 SIV+ animals while lower concentrations of MPO were detected in 7/7 SIV- animals (**Figure**

262   **4C**). Post-ZIKV infection, concentrations of plasma MPO continue to be significantly higher in

263   SIV+ZIKV+ animals in comparison to SIV-ZIKV+ animals (**Figure 4C**). These data suggest that

264   neutrophils are more inflammatory during SIV infection and there is an impairment of neutrophil

265   recruitment to the blood and impaired trafficking to gastrointestinal tissues post-ZIKV.

266

267   ***SIV-ZIKV co-infection induces chronic innate immune activation.***

268   The inflammatory response to ZIKV in the plasma was evaluated using a multiplex

269   immunoassay. In both groups, ZIKV induced pro-inflammatory responses, characterized by

270   transient increases in interleukin-1 receptor agonist (IL-1RA), monocyte chemoattractant protein-

271   1 (MCP-1), and vascular endothelial growth factor A (VEGF-A) (**Supplemental Figure 11**), with

272   no major differences between groups. Although we found no evidence of ZIKV infection in

273   neuronal tissue, neuroinflammation was evaluated in longitudinal CSF specimens. CSF

274   concentrations of sCD14, a marker of neuroinflammation, did not change with ZIKV infection in

275   either group (**Supplemental Figure 5B**). IL-1RA, IL-6, IL-8, and VEGF-A were elevated in several

276   animals across groups at varying timepoints (**Supplemental Figure 11**). Transient increases in

277   IL-8 were detected in the CSF of a few SIV-ZIKV+ animals after ZIKV infection, which is evidence

278   of neuroinflammation. At necropsy, two animals in the ZIKV+ group (L07201 and Z08062) had

279   mild, multifocal demyelination and axonal loss in the brainstem, which may be a result of

280   neuroinflammation despite no evidence of ZIKV infection at this site (**Supplemental Table 2, 8**).

281   Overall, no significant differences between SIV+ vs SIV- groups were found for any analytes

282   detected in plasma or CSF during ZIKV infection, suggestive that SIV infection does not enhance

283   ZIKV-induced systemic inflammation or neuroinflammation.

284   To further examine SIV effects on immune responses to ZIKV, we performed targeted

285   gene expression analysis on longitudinal PBMC specimens collected post-ZIKV infection using a

286   custom-built NanoString Code Set for interrogating 64 genes marking innate activation,

287   inflammatory and interferon (IFN) responses. Changes in gene expression were determined at

288   each time-point post challenge in comparison to uninfected timepoints. Gene expression was not

289   significantly changed 7 weeks post-SIV infection relative to naïve PBMC. This indicated that while

290   SIV infection stimulated gene expression, the changes just prior to ZIKV challenge were not

291   significantly different from baseline levels. Following ZIKV challenge, a total of 23 genes were

292   significantly differentially expressed (22 upregulated and 1 downregulated), 14 genes in SIV-

293   ZIKV+ (13 up and 1 down), 19 genes in SIV+ZIKV+ (19 up), and 10 genes in both groups (10 up)

294   **(Figure 5B, Supplemental Table 5).** ZIKV induced robust innate immune gene activation in SIV-

295   ZIKV+ animals during acute infection (2-4 dpi), with the expression of most genes returning to

296   baseline by 7 dpi (**Figure 5A**). The kinetics of the gene expression mirrors peak ZIKV viremia

297   (median 3 dpi) and time to viral clearance (median 7 dpi). While these innate immune genes were

298   also strongly upregulated in SIV+ZIKV+ co-infected animals during acute infection (2-4 dpi), in

299   contrast to the SIV-ZIKV+ group, the gene signature was maintained throughout infection and

300   remained highly expressed 7-21 dpi. The kinetics of gene expression during SIV+ZIKV+ co-

301   infection corresponds to the shift in peak ZIKV viremia (median 4 dpi) and viral clearance (median

302   10 dpi). We also found that the expression of 10 genes were significantly different between

303   SIV+ZIKV+ and SIV-ZIKV+ animals, primarily at 14 and 21 dpi, and predominantly consisted of

304   genes associated with type I IFN signaling and ZIKV viral control (*ISG15, IFIT1, MX1, ISG20,*

305   *IRF7*) (**Figure 5C, Supplemental Table 6**). These data demonstrate that SIV-ZIKV co-infection

306   leads to persistent upregulation of genes associated with inflammation and innate immune

307   activation in whole blood. This chronic hyperactivated innate immune state in response to ZIKV

308   co-infection is likely a contributing factor in the impaired peripheral ZIKV clearance and ZIKV

309   persistence in tissues.

310

311   **Discussion**

312   In this study, we aimed to determine whether HIV-induced immunosuppression impacts ZIKV

313   pathogenesis and investigated this using *in vitro* and *in vivo* models of SIV-ZIKV co-infection. We

314   identified that peripheral ZIKV cellular targets, including CD16+ monocytes, increase during acute

315   infection but contract to pre-infection levels during early chronic stages of SIV infection (**Figure

316   6**). Despite AXL being an important cellular receptor of ZIKV infection, we found no change in

317   AXL expression on monocytes in whole blood or tissues of SIV+ animals following ZIKV

318   challenge. This indicates that enhanced ZIKV persistence during SIV infection is unlikely to be

319   caused by increased receptor engagement on cellular targets. Interestingly, PBMC from acutely

320   SIV infected NHP exhibit an anti-viral gene expression profile that renders the cells refractory to

321   ZIKV co-infection *in vitro.* We also demonstrated *in vivo* that SIV infection modulates the innate

322   and adaptive immune response to ZIKV co-infection and creates a hyper inflammatory state that

13

323   could contribute to prolonged viremia and impaired viral clearance from the tissues, particularly

324   in the gastrointestinal tract (**Figure 6**). This study further implies that PLWH or other

325   immunocompromised individuals co-infected with ZIKV have the potential for longer ZIKV

326   transmission periods.

327   The clinical impact of HIV co-infection on flavivirus infection remains unclear. For example,

328   some studies report less, while others report more severe disease during DENV-HIV co-

329   infection(44-46). ZIKV infection during pregnancy in women living with HIV is of great concern:

330   one study reported 12% of ZIKV exposed infants to women living with HIV had CNS

331   abnormalities(47), as compared to reports of 5-8% in ZIKV exposed infants from HIV- women(48),

332   indicating there may be greater risks of neuropathologies in HIV-ZIKV exposed infants. These

333   flavivirus co-infection studies in PLWH are limited by low patient numbers, inconsistent

334   incorporation of ART and HIV disease status, and parameters are primarily restricted to

335   measurements in the blood. Studies examining ZIKV infection in SIV or SHIV infected NHP have

336   helped fill this clinical gap. One study found that pregnant female macaques with treated SIV

337   infection (SIVmac239), had similar rates of pregnancy loss due to ZIKV exposure (ZIKV-DAK)

338   when compared to SIV naïve animals(49). Whether rates of fetal loss are similar in those with

339   untreated SIV infection remains an area of potential future investigation. Two studies have

340   investigated ZIKV co-infection in non-pregnant rhesus macaques with untreated SIV/SHIV

341   infection(50, 51). Bidokhti et al., reported no differences in ZIKV virema with SIV/SHIV infection;

342   however, interpretations from this study are limited by low animal numbers and a lack of

343   contemporaneous controls(51). Notably and similar to our findings here, Vinton et al., observed

344   delayed peak ZIKV viremia and clearance in SIV-infected rhesus(50). Higher levels of ZIKV RNA

345   were detected in lymph nodes from SIV+ rhesus at 27 dpi(50), and while we detected persistence

346   of ZIKV in SIV+ and SIV- pigtail macaque, we found no significant differences in viral burden

347   between groups. These differences may be due, in part, to the sensitivities of the methods used,

348   fluorescence in situ hybridization in Vinton et al., versus qRT-PCR in our study. Notably, our study

349 uniquely provides additional insight that SIV infection promotes ZIKV persistence in

350 gastrointestinal tissues, a tissue compartment that was not reported in previous studies. Major

351 differences in experimental design between previous reports and our study here include 1)

352 different species (rhesus versus pigtail macaques), 2) the time of ZIKV co-infection (3 weeks or

353 6-7 months post-SIV versus 9 weeks post-SIV), and 3) strain of ZIKV (Nicaragua/2016 and

354 PRVABC59 versus Brazil_2015). Collectively, our study and that of Vinton et. al suggest that

355 untreated acute SIV infection alters ZIKV viral kinetics and enhances ZIKV persistence or viral

356 burden in tissues. This suggests that immunocompromised individuals may have longer ZIKV

357 transmission periods or altered disease pathogenesis and should be primary candidates for ZIKV

358 vaccines.

359 ZIKV and West Nile Virus (WNV) can invade the central nervous system, yet the

360 mechanisms of neuropathogenesis are not well understood[52, 53]. ZIKV RNA in the CSF or

361 brain is detected infrequently but consistently reported in rhesus and cynomolgous macaques[20,

362 25, 54-56]. In contrast, ZIKV RNA in the CSF or CNS was not detected in adult pigtail macaques

363 reported here and in our previous report[24]. This suggests that the frequency or severity of ZIKV

364 neuroinvasion may vary between macaque species and that different host factors could play a

365 role. Evidence for neuroinflammation is reported in ZIKV infected NHP, even when ZIKV RNA is

366 undetectable in the CSF[54, 57-59]. Increases in inflammatory infiltrates into the CSF of ZIKV

367 infected rhesus, including IL-15, MCP-1, G-CSF, and CXCL12, are previously reported[57, 58].

368 Here, we also observed that IL-1RA, IL-6, and IL-8 concentrations were elevated in the CSF;

369 however, these responses were highly variable between animals. It is plausible that the

370 differences in observed cytokine milieus between our study in pigtail macaques and those in

371 rhesus macaques are due to assay sensitivities and cross-reactivity levels across assays.

372 However, this could point to potential differences in neuroinflammatory responses between

373 macaque species. In PLWH, increased WNV neuroinvasion occurs[60-62] and supports that HIV-

374 ZIKV co-infection could similarly result in increased targeting of ZIKV to the CNS, resulting in

15

375 higher rates of neurological pathologies. Our studies here provide no evidence that SIV infection

376 promotes increased ZIKV neuroinvasion or neuroinflammation, however additional studies in

377 other NHP species are needed to fully assess this risk.

378 Many promising ZIKV vaccine candidates in the pre-clinical pipeline rely on the induction

379 of antibodies and T-cells to mediate protection(63). Studies in NHP revealed that CD8 T-cells are

380 not required for protection against primary or secondary ZIKV infections(25, 64). Another study in

381 NHP further showed that the impaired generation of anti-flavivirus humoral responses in CD4

382 depleted macaques infected with DENV and ZIKV, shapes the quality of responses to a tertiary

383 flavivirus exposure(65). Here, our study is in congruence with Vinton et al.(50), and demonstrates

384 that the generation of anti-ZIKV adaptive immunity is impaired in SIV infected animals that exhibit

385 CD4 immunodeficiency. Further studies are needed to elucidate whether the immune responses

386 generated during CD4 immunosuppression are sufficient for protection against homologous

387 and/or heterologous re-exposure to ZIKV. This will improve our ability to identify groups at risk for

388 re-infection and to create effective vaccines in various states of immunosuppression, including

389 those for the elderly, pregnant women, and immunocompromised individuals.

390 The innate immune response is the primary defense against flavivirus infection, but if

391 dysregulated or uncontrolled, it can lead to enhanced viral pathogenesis. This dichotomous role

392 is further complicated during flavivirus infection, as innate immune cells, including monocytes and

393 dendritic cells, are targets of ZIKV, WNV, and DENV infection. In our *in vitro* co-infection model,

394 we found that PBMC from SIV infected animals were less permissive to ZIKV infection, and in our

395 *in vivo* model, ZIKV replication was delayed in the periphery. Initially cells from

396 immunosuppressed individuals may be less permissive to ZIKV infection due to an antiviral state

397 and this may contribute to a slower establishment of ZIKV infection. However, once established,

398 the ability to recruit immune cells critical for clearing the ZIKV infection is impaired and

399 dysregulated during immunosuppression, promoting dissemination and persistence of ZIKV in the

400 tissues, most notably the gastrointestinal tract (**Figure 6**). Previously, we reported that the

16

401   infiltration of neutrophils and CD16- classical monocytes/macrophages into tissues may be

402   important for controlling Zika virus replication(24). Here, we further corroborate this finding and

403   demonstrate that CD16+ inflammatory monocytes/macrophages, but not CD16-

404   monocytes/macrophages nor neutrophils, traffick into the tissues of SIV+ZIKV+ animals and

405   correspond to ZIKV persistence (**Figure 6**). Prolonged innate immune activation is a hallmark of

406   chronic infections, including HIV, but can also be observed following acute viral infections.

407   Notably, SARS-CoV-2 infection is predominantly an acute infection, yet in some individuals

408   SARS-CoV-2 virus can persist in the tissues and/or lead to post-acute sequelae of COVID-19

409   (PASC)(66). PASC is associated with persistent immune activation and PLWH are at greater risk

410   for PASC(67). This suggests that chronic innate immune activation can be a major driver in

411   promoting viral persistence. Our study supports the possibility that chronic innate immune

412   activation could similarly contribute to ZIKV persistence. Due to the variability of immune

413   responses and disease outcomes in our study, additional studies are needed to elucidate the

414   immune mechanisms contributing to flavivirus persistence in states of immunosuppression.

415

416   **Figure Legends**

417   **Figure 1. PBMC from SIV-infected PTM are less permissive to *in vitro* ZIKV infection.** (**A**-**B**)

418   Peripheral blood mononuclear cells (PBMC) were isolated from pigtail macaques prior to and at

419   2 and 6 weeks post-SIV infection and infected *in vitro* with ZIKV Brazil at a multiplicity of infection

420   (MOI) of 2. Cells and supernatant were harvested 4, 24, and 48 hours post-infection. (**A**)

421   Quantitative real-time PCR (qRT-PCR) for ZIKV RNA in PBMC. (**B**) Plaque assay for infectious

422   virus. (**A-B**) Medians with interquartile ranges are shown. Kruskal-Wallis test versus pre-SIV

423   levels, p-values * ≤ 0.05. (**C**) Frequency of CD16+CD14+ monocytes and macrophages (top

424   panel) and dendritic cells lower panel) in blood from uninfected and SIV-infected pigtail

425   macaques. Wilcoxon matched-pairs signed rank test, p-values ≤ 0.05 considered significant. (**D**)

17

Gene expression of PBMC in blood at Week 2 post-SIV (top panel) and Week 6 post-SIV (bottom panel). t-test between each time-point relative to Pre-SIV, p-values *<0.01 shown by orange dots.

Figure 2. ZIKV viremia is delayed and protracted and ZIKV viral burden more persistent in gastrointestinal tissues in SIV-infected macaques. (**A**) Study design of longitudinal blood and tissue sampling following SIV and ZIKV infections in pigtail macaques. Initially n=7/group were infected with ZIKV, however 1 animal in the SIV+ group displayed no evidence of ZIKV replication and thus was excluded from all post-ZIKV analysis. (**B**) Quantitative real-time PCR (qRT-PCR) for ZIKV RNA in longitudinal samples from plasma, peripheral lymph node (PLN), rectal biopsies, and rectal cytobrush until necropsy (Nx). Virus was not detected in any longitudinal cerebrospinal fluid (CSF). (**C**) ZIKV RNA in tissues collected at necropsy 24-28 DPI. Virus was not detected in brain tissue (brainstem, hippocampus, frontal lobe, parietal lobe, and occipital lobe) of any animal.

Figure 3. SIV infection may impair anti-ZIKV immunity. (**A**) Longitudinal plasma concentrations of anti-ZIKV envelope IgG as determined by ELISA. AUCs were calculated from day 10 to 28. Medians with interquartile ranges are displayed. (**B**) Zika virus neutralization antibody titers (NT50 values) evaluated at necropsy. The line represents the median and the dotted line represents is the limit of detection. (**A-B**) Mann-Whitney test comparison between groups.

Figure 4. Post-ZIKV recruitment of CD16+ monocytes and macrophages is dampened in the periphery, but enhanced in tissues in SIV-infected macaques. (**A**) Frequency of CD16+CD14+ monocytes and macrophages in blood (left panel), rectum (center panel), and peripheral lymph node (right panel) after ZIKV infection. (**B**) Frequency of neutrophils in blood after ZIKV infection. (**C**) Concentration of myeloperoxidase (MPO) in plasma as measured by ELISA. (**A-**

451   **C**) Medians with interquartile ranges are shown. Mann-Whitney test between group, p-values * ≤

452   0.05.

453

454   **Figure 5: SIV-ZIKV co-infection induces chronic innate immune activation in PBMC**. (**A**)

455   Heatmap showing the LFC expression of 23 genes that were significantly different (*p*-value<0.01)

456   in at least one time point and one group. LFC expression for the SIV+ZIKV+ group is relative to

457   pre-SIV (Wk-3). LCF expression for the SIV-ZIKV+ group is relative to pre-ZIKV (D-14). Genes'

458   LFCs were clustered using Pearson and Ward.D2. (**B**) Venn diagram of shared and unique genes

459   that were significantly upregulated post-ZIKV. (**C**) Line plots of select gene kinetics representing

460   the mean of all SIV+ZIKV+ (red) or SIV-ZIKV+ (black) animals. The log2 normalized counts are

461   plotted at each time point. The line represents the mean and the standard error is shown as the

462   confidence interval around the mean. p-values *<0.01 indicates a significant difference between

463   SIV+ZIKV+ and or SIV-ZIKV+ at a specified time point.

464

465   **Figure 6: Model of innate immune impairment and ZIKV persistence during SIV infection**.

466   The model depicts impaired induction of monocyte recruitment, presence of inflammatory

467   neutrophils, and chronic immune activation in the periphery. These findings, coupled with the

468   absence of anti-ZIKV IgG, suggest a mechanism for delayed clearance of ZIKV viremia. ZIKV

469   persistence in gastrointestinal tissues is enhanced in an immunocompromised state and the

470   preferential recruitment of CD16+ monocytes/macrophages into tissue may be a contributing

471   mechanism. Created with biorender.com.

Materials & Methods

Study Design and Animal Welfare

A total of 14 male and female pigtail macaques (aged 4-11 years, 6-13 kg) were used. **Supplemental Table 1** details animal characteristics, including MHC haplotypes and experimental vaccination history. Prior to enrollment, all animals were pre-screened and seronegative for the presence of antibodies to West Nile, dengue, and Zika viruses. At least 2 months prior to enrollment into the study, eight animals were previously enrolled in studies in which they received an experimental hepatitis B virus (HBV) vaccine consisting of a combination of CD180 targeted DNA and recombinant protein vaccines comprised of HBV core and surface antigens(27) and/or a replicating RNA COVID-19 vaccine(28) (**Supplemental Table 1**) and were evenly distributed between the control and experimental groups. Seven pigtail macaques were infected intravenously with 10,000 infectious units (I.U.) of SIVmac239M(29) (gift from Dr. Brandon Keele, AIDS and Cancer Virus Program, Frederick National Laboratory for Cancer Research) and then co-infected with ZIKV at 9 weeks. All animals were subject to a Simian AIDS monitoring protocol as defined by the WaNPRC guidelines(30). All animals were inoculated with 5×10^5 PFU of the Brazil_2015_MG strain of ZIKV (GenBank: KX811222.1), as previously described(24). ZIKV RNA was not detected in any specimen tested at any timepoint in one animal in the SIV-infected group (Z14109); therefore, this animal was excluded from all post-ZIKV analysis. All animals were euthanized at the study endpoint at 4 weeks post-ZIKV infection under deep anesthesia, in accordance with the 2007 American Veterinary Medical Association Guidelines on Euthanasia, by administration of Euthasol® (Virbac Corp., Houston, TX). As previously described(24), all animals were housed at the Washington National Primate Research Center (WaNPRC), an accredited facility the American Association for the Accreditation of Laboratory Animal Care International (AAALAC). All animal procedures were approved by the University of Washington's Institutional Animal Care and Use Committee (IACUC) and were collected and processed as previously described(24) and according to the schematic in **Figure**

498   **2A**. Animals were observed daily and full physical exams were conducted at each experimental

499   timepoint, as previously described(24).

500

501   *Simian AIDS Measurements*

502   SIV plasma viremia was evaluated by quantitative real time reverse transcription polymerase

503   chain reaction (RT-PCR) by the Virology and Immunology Core at the WaNPRC, as previously

504   described(30), and by the NIAID DAIDS Nonhuman Primate Core Virology Laboratory (NHPCVL)

505   for AIDS Vaccine Research and Development Contract. Complete blood counts (CBC) and serum

506   chemistries were performed by the Research Testing Service (RTS) at the University of

507   Washington Department of Laboratory Medicine. Peripheral CD4 counts were determined from

508   CBC using flow cytometry-based methods by the Virology and Immunology Core at the WaNPRC,

509   as previously described(31).

510

511   *Cell culture and virus stock*

512   Peripheral blood mononuclear cells (PBMC) were isolated from NHP whole blood collected pre-

513   SIV inoculation (Wk-3) and at weeks 2 and 6 post-SIV inoculation, as previously described(24).

514   PBMC were maintained in RPMI medium supplemented with 10% fetal bovine serum (FBS;

515   HyClone), 2 mM L-glutamine, 5 mM sodium pyruvate, 1x Antibiotic Antimycotic Solution, and 10

516   mM HEPES (cRPMI; complete RPMI). RPMI medium used for the ZIKV inoculation was

517   supplemented with 1% FBS, 2 mM L-glutamine, 5 mM sodium pyruvate, 1x Antibiotic Antimycotic

518   Solution, and 10 mM HEPES (iRPMI; infection RPMI). Vero cells (WHO, Geneva, Switzerland)

519   were cultured in complete Dulbecco's modified Eagle medium (cDMEM) supplemented with 10%

520   FBS, 2 mM L-glutamine, 5 mM sodium pyruvate, 1x Antibiotic Antimycotic Solution, 10 mM

521   HEPES and 1X non-essential amino acids. Vero cells tested negative for mycoplasma

522   contamination. All cells were maintained in a 37°C incubator with 5% CO_2. Brazil Zika virus stock

523   (GenBank: KX811222.1) was used for the PBMC inoculation.

21

524

ZIKV infection of PBMC

526   Following overnight incubation, PBMC cell suspensions were prepared, and the cell concentration

527   and viability measured using the Countess 3 Automated Cell Counter (ThermoFisher Scientific).

528   Approximately 6×10^6 PBMC were inoculated with ZIKV at an MOI of 2 in a total volume of 200

529   µL RPMI infection medium (iRPMI) at 37°C for 2 hours (h). Cells were gently mixed by pipetting

530   at 20 minute (min) intervals during incubation. After 2 h, the cells were spun at 300 relative

531   centrifugal force (rcf) for 3 min at RT and the inoculum carefully removed without disturbing the

532   cell pellet. The cells were washed with 300 µl iRPMI and then resuspended in pre-warmed

533   complete RPMI (cRPMI). A total of 5×10^5 PBMC were added to each well of a 24-well plate

534   containing 1 mL of cRPMI. The plates were returned to 37°C and incubated until the designated

535   time-point for sample collection. At 4, 24, and 48 h post-ZIKV inoculation, supernatants were

536   collected and spun at 300 rcf for 3 min at 4°C. 100 µL Versene solution (ThermoFisher Scientific)

537   was added to each well to dislodge adherent cells from the TC plate. The clarified supernatant

538   was transferred to a new tube and banked at -80°C until further processing by plaque assay or

539   qRT-PCR assay. The Versene solution containing PBMC was added to the PMBC cell pellet from

540   the supernatant and then spun at 300 rcf for 3 min at 4°C. The supernatant was carefully removed

541   from the cell pellet and discarded. The cell pellet was then resuspended in 700 µL QIAzol for RNA

542   analysis.

543

Plaque assay

545   Vero cells (WHO, Geneva, Switzerland) were seeded at a density of 5×10^5 cells per well in 6-

546   well plates. The next day, the medium was removed from the monolayers and 200 µL of 10-fold

547   serial dilutions of virus-containing supernatant in DMEM containing 2% FBS added to respective

548   wells in duplicate. Vero cell monolayers were incubated at 37°C for 2 h, with rocking at 15 min

22

549   intervals. Monolayers were overlaid with 1% low-melting point SeaPlaque® agarose (Lonza), set

550   at 4°C for at least 20 min, and then returned to the 37°C incubator. Plaques were visualized and

551   counted 4 days later by crystal violet staining.

552

553   *NanoString nCounter Assay and Gene Analysis*

554   The NanoString nCounter platform (NanoString, Seattle, WA, USA) was used to quantify mRNA

555   counts in PBMC processed from whole blood at pre- and post-SIV and ZIKV infection time-points.

556   RNA was isolated from cryopreserved PBMC samples collected at pre-SIV inoculation (Wk -3), 2

557   and 6 weeks post-SIV using the miRNeasy Mini Kit (QIAGEN). RNA was isolated from 1-2 x 10^6

558   PBMC resuspended in 700 µl QIAzol collected at week 7/Day -14 pre-ZIKV inoculation, and at

559   days 2, 4, 7, 10, 14 and 21 post-ZIKV challenge using the miRNeasy Micro Kit (QIAGEN). From

560   each sample, 100 ng RNA was loaded in accordance with manufacturer's instructions for targeted

561   expression with 2 custom-built curated NanoString Human Panels of 44 and 60 genes of interest

562   which both represent gene biomarkers of innate immune activation and response, interferon

563   response, and inflammatory response. Due to the small number of genes represented on the

564   Code Set, nCounter data normalization was performed using a method which calculates a ratio

565   between genes of interest to housekeeping genes(32). The ratio is calculated by dividing the

566   counts of the genes of interest by the geometric mean of 4 housekeeping genes which have the

567   lowest coefficient of variance across all samples. This is done for each sample independently,

568   which generates normalized expression for the genes of interest. Significant differences (nominal

569   *P*-val <0.01) were determined between baseline and infection time points for each group and

570   between groups at each time point.

571

572   *Histology*

573   At necropsy representative samples of all tissues and organs were collected in formalin and

574   after fixation were paraffin embedded and sectioned at 3-5 µm. For basic histology, sections

23

575   were stained with hematoxylin and eosin. All histological findings are summarized in

576   **Supplemental Table 2***.

577

578   *Immunophenotyping*

579   Isolated PBMC, rectal and peripheral lymph node biopsy cells were assessed for viability with a

580   live/dead stain (Life Technologies) and stained with a panel of antibodies, details described in

581   **Supplementary Table 3,** in brilliant stain buffer (BD Biosciences) to identify innate immune cells

582   as previously described(24). Paraformaldehyde fixed cells were acquired on a LSRII (BD

583   Biosciences) using FACS Diva software (version 8). Samples were analyzed using FlowJo

584   software version 10.8.1 (FlowJo, LLC). All events were first gated on FSC singlets, CD45$^+$

585   leukocytes, live, and then cells according to FSC-A and SSC-A profiles. Immune cells were

586   identified as follows: plasmacytoid dendritic cells (DCs) (CD20$^-$CD3$^-$HLA-DR$^+$CD14$^-$

587   CD123$^+$CD11c$^-$), myeloid DCs (CD20$^-$CD3$^-$HLA-DR$^+$CD14$^-$ CD123$^-$CD11c$^+$), monocytes (CD20$^-$

588   CD3$^-$HLA-DR$^+$CD14$^+$CD16$^{+/-}$), and neutrophils (CD3$^-$CD11b$^+$CD14$^+$SSC-A^{Hi}). AXL positive cells

589   were identified after FMO subtraction and meeting a cellular threshold ($\geq$100 cells/gate).

590

591   *Multiplex Bioassay*

592   Cytokine and chemokine levels in plasma and cerebrospinal fluid (CSF) were analyzed using a

593   custom nonhuman primate ProcartaPlex 24-plex immunoassay (ThermoFisher Scientific), per the

594   manufacturer's protocol. The levels of the analytes were assessed on a Bio-Plex 200 system (Bio-

595   Rad) and analyzed per the manufacturer's protocol.

596

597   *ZIKV RNA Quantification*

598   Viral RNA load was assessed in plasma, CSF, rectal cytobrush supernatant, and tissues using a

599   ZIKV-specific RT-qPCR assay, as previously described(24). RNA was isolated from plasma and

600   rectal cytobrush supernatant collected pre-challenge and at 1, 2, 3, 4, 7, 10, 14 and 21 days post-

24

601 infection (dpi) and at necropsy (24-28 dpi). RNA was isolated from CSF collected pre-challenge

602 and at days 4, 7 and 21 post-challenge and at necropsy (24-28 dpi). Rectal and PLN biopsy

603 tissues were collected pre-challenge and at days 7 and 21 post-challenge and lymphoid and gut

604 tissues collected at necropsy (24-28 dpi). The iScript Select cDNA Synthesis Kit (Bio-Rad) was

605 used for gene-specific cDNA synthesis and cDNAs were quantified on a QuantStudio Real-Time

606 PCR System (ThermoFisher Scientific). Ct values <39 in at least 2 of the triplicates and falling

607 within the standard curve determined from diluted known quantities of ZIKV genome were

608 considered positive.

609

610 *Gut integrity and neuroinflammation*

611 Plasma and/or CSF quantification by ELISA of human soluble CD14 (sCD14), human fatty acid

612 binding protein 2 (FABP2) (Fisher Scientific, Waltham, MA) or human LPS binding protein (LBP)

613 (Biometec, Germany) was performed per the manufacturer's instruction. Plasma was diluted as

614 follows: 1:200 (sCD14), 1:2 (FABP2), or 1:3 (LBP). CSF was diluted 1:5 (sCD14). Results were

615 analyzed using Prism version 8.4.3 (GraphPad) and using a four- or five- parameter logistic (4-

616 or 5-PL) function for fitting standard curves.

617

618 *Anti-ZIKV IgG Quantification*

619 NHP sera and/or plasma samples were assessed for anti-ZIKV envelope (E) IgG binding titers by

620 an Enzyme-Linked Immunosorbent Assay (ELISA). Purified NHP IgG (MyBioSource

621 MBS539659) was serially diluted to establish a range of IgG standards. ZIKV E protein (Fitzgerald

622 Industries International, 30-1932) was diluted to 0.5 μg/mL and was used as the capture antigen.

623 Capture antigen and IgG standards were coated overnight on high-binding 96-well plates (Costar

624 3590) to produce test and standard wells, respectively. All wells were subsequently blocked in

625 blocking buffer (5% w/v nonfat dried milk (Bio-Rad Laboratories 1706404) and 0.05% v/v Tween-

626 20 in PBS). Samples were diluted 1:100, 1:200, and/or 1:400 and tested in triplicate. NHP IgG

627 standard and test wells were probed by a goat anti-monkey IgG antibody conjugated to

628 Horseradish peroxidase (HRP) (Abcam ab112767). SureBlue Reserve TMB substrate (KPL) was

629 added to all wells to initiate a color change reaction catalyzed by HRP. Reaction was stopped

630 after 30 minutes with 1N HCl (VWR) and absorbance at 450nm (Abs_{450}) was measured on an

631 EMax plate reader (Molecular Devices). Abs_{450} of standard wells were used to produce a 5PL

632 logistic fit (GraphPad Prism). Abs_{450} of test wells were converted to μg/mL of anti-ZIKV E IgG

633 binding titers via the 5PL logistic fit.

634

635 *Plaque reduction neutralization test (PRNT)*

636 NHP sera collected pre-challenge (Day -14) and at necropsy (24-28 dpi) were tested in PRNT

637 assay for neutralizing antibody production, as previously described(33). The PRNT assay was

638 performed using serial two-fold dilutions of the serum samples. The highest serum dilution

639 reducing plaque numbers by 50% ($PRNT_{50}$) were determined with a limit of detection (LOD) of

640 1:50. The assay was repeated twice in triplicate using the ZIKV Brazil 2015 virus.

641

642 *Statistical analysis*

643 Non-parametric statistical methods were employed for all comparisons, unless otherwise noted.

644 Specifically, Kruskal-Wallis tests were used for comparisons across timepoints in *in vitro*

645 experiments, paired Wilcoxon tests were used to evaluate cell fraction differences to baseline at

646 each timepoint, and Mann-Whitney tests were used to compare continuous values across groups.

647 All analyses were conducted using two-sided tests at the 0.05 level. Analyses were conducted in

648 Prism version 8.4.3h (GraphPad). Significant differences (nominal *P*-val <0.01) in gene

649 expression were determined using a t test that compared baseline and infection time points for

650 each group and between groups at each time point.

651

652 *Data Availability*

653   The data that support the findings of this study are available from the corresponding author upon

654   reasonable   request.   The   NanoString   nCounter   analysis   code   is   available   at

655   https://github.com/galelab/OConnor_SIV-ZIKV_coinfection.

682

Author Contributions

JTG, MAO, MG, DHF, and MAO designed and coordinated the studies. TBL, KV, SN, KH, EB,

AH, and MAO led the immunological assays and analysis. JTG, KV, SN, PK, and MAO led the

virologic assays and analysis. JTG, LSW, and JD led the transcriptomic data generation and

analysis. NI, CA, SW, RM, and KAG led specimen collection and RM and KAG led the clinical

care of the animals. PTE assisted with the statistical analysis. JTG and MAO led the studies,

interpreted the results, and wrote the paper with all co-authors.

690

References

1.   Ishikawa T, Yamanaka A, Konishi E. A review of successful flavivirus vaccines and the problems with those flaviviruses for which vaccines are not yet available. Vaccine. 2014;32(12):1326-37.
2.   Veit O, Niedrig M, Chapuis-Taillard C, Cavassini M, Mossdorf E, Schmid P, et al. Immunogenicity and safety of yellow fever vaccination for 102 HIV-infected patients. Clin Infect Dis. 2009;48(5):659-66.
3.   Thomas RE, Lorenzetti DL, Spragins W, Jackson D, Williamson T. The safety of yellow fever vaccine 17D or 17DD in children, pregnant women, HIV+ individuals, and older persons: systematic review. Am J Trop Med Hyg. 2012;86(2):359-72.
4.   (CDC) CfDCaP. CDC Yellow Book 2024, Health Information for International Travel2024. 912 p.
5.   D'Ortenzio E, Matheron S, Yazdanpanah Y, de Lamballerie X, Hubert B, Piorkowski G, et al. Evidence of Sexual Transmission of Zika Virus. N Engl J Med. 2016;374(22):2195-8.
6.   Davidson A, Slavinski S, Komoto K, Rakeman J, Weiss D. Suspected Female-to-Male Sexual Transmission of Zika Virus - New York City, 2016. MMWR Morb Mortal Wkly Rep. 2016;65(28):716-7.
7.   Oliveira Souto I, Alejo-Cancho I, Gascón Brustenga J, Peiró Mestres A, Muñoz Gutiérrez J, Martínez Yoldi MJ. Persistence of Zika virus in semen 93 days after the onset of symptoms. Enferm Infecc Microbiol Clin (Engl Ed). 2018;36(1):21-3.
8.   Brasil P, Sequeira PC, Freitas AD, Zogbi HE, Calvet GA, de Souza RV, et al. Guillain-Barré syndrome associated with Zika virus infection. Lancet. 2016;387(10026):1482.
9.   Sousa AQ, Cavalcante DIM, Franco LM, Araújo FMC, Sousa ET, Valença-Junior JT, et al. Postmortem Findings for 7 Neonates with Congenital Zika Virus Infection. Emerg Infect Dis. 2017;23(7):1164-7.
10.   Moore CA, Staples JE, Dobyns WB, Pessoa A, Ventura CV, Fonseca EB, et al. Characterizing the Pattern of Anomalies in Congenital Zika Syndrome for Pediatric Clinicians. JAMA Pediatr. 2017;171(3):288-95.
11.   Nielsen-Saines K, Brasil P, Kerin T, Vasconcelos Z, Gabaglia CR, Damasceno L, et al. Delayed childhood neurodevelopment and neurosensory alterations in the second year of life in a prospective cohort of ZIKV-exposed children. Nat Med. 2019;25(8):1213-7.

723 12.   Neelam V, Woodworth KR, Chang DJ, Roth NM, Reynolds MR, Akosa A, et al.
724 Outcomes up to age 36 months after congenital Zika virus infection-U.S. states. Pediatr Res.
725 2024;95(2):558-65.
726 13.   Mulkey SB, Williams ME, Peyton C, Arroyave-Wessel M, Berl MM, Cure C, et al.
727 Understanding the multidimensional neurodevelopmental outcomes in children after congenital
728 Zika virus exposure. Pediatr Res. 2024.
729 14.   Dudley DM, Aliota MT, Mohr EL, Weiler AM, Lehrer-Brey G, Weisgrau KL, et al. A
730 rhesus macaque model of Asian-lineage Zika virus infection. Nat Commun. 2016;7:12204.
731 15.   Steinbach RJ, Haese NN, Smith JL, Colgin LMA, MacAllister RP, Greene JM, et al. A
732 neonatal nonhuman primate model of gestational Zika virus infection with evidence of
733 microencephaly, seizures and cardiomyopathy. PLoS One. 2020;15(1):e0227676.
734 16.   Dudley DM, Van Rompay KK, Coffey LL, Ardeshir A, Keesler RI, Bliss-Moreau E, et al.
735 Miscarriage and stillbirth following maternal Zika virus infection in nonhuman primates. Nat Med.
736 2018;24(8):1104-7.
737 17.   Hirsch AJ, Roberts VHJ, Grigsby PL, Haese N, Schabel MC, Wang X, et al. Zika virus
738 infection in pregnant rhesus macaques causes placental dysfunction and immunopathology. Nat
739 Commun. 2018;9(1):263.
740 18.   Adams Waldorf KM, Stencel-Baerenwald JE, Kapur RP, Studholme C, Boldenow E,
741 Vornhagen J, et al. Fetal brain lesions after subcutaneous inoculation of Zika virus in a pregnant
742 nonhuman primate. Nat Med. 2016;22(11):1256-9.
743 19.   Tisoncik-Go J, Stokes C, Whitmore LS, Newhouse DJ, Voss K, Gustin A, et al.
744 Disruption of myelin structure and oligodendrocyte maturation in a pigtail macaque model of
745 congenital Zika infection. bioRxiv. 2023.
746 20.   Osuna CE, Lim SY, Deleage C, Griffin BD, Stein D, Schroeder LT, et al. Zika viral
747 dynamics and shedding in rhesus and cynomolgus macaques. Nat Med. 2016;22(12):1448-55.
748 21.   Moreno GK, Newman CM, Koenig MR, Mohns MS, Weiler AM, Rybarczyk S, et al. Long-
749 Term Protection of Rhesus Macaques from Zika Virus Reinfection. J Virol. 2020;94(5).
750 22.   Foo SS, Chen W, Chan Y, Bowman JW, Chang LC, Choi Y, et al. Asian Zika virus
751 strains target CD14(+) blood monocytes and induce M2-skewed immunosuppression during
752 pregnancy. Nat Microbiol. 2017;2(11):1558-70.
753 23.   Michlmayr D, Andrade P, Gonzalez K, Balmaseda A, Harris E. CD14(+)CD16(+)
754 monocytes are the main target of Zika virus infection in peripheral blood mononuclear cells in a
755 paediatric study in Nicaragua. Nat Microbiol. 2017;2(11):1462-70.
756 24.   O'Connor MA, Tisoncik-Go J, Lewis TB, Miller CJ, Bratt D, Moats CR, et al. Early cellular
757 innate immune responses drive Zika viral persistence and tissue tropism in pigtail macaques.
758 Nat Commun. 2018;9(1):3371.
759 25.   Schouest B, Fahlberg M, Scheef EA, Ward MJ, Headrick K, Szeltner DM, et al. Immune
760 outcomes of Zika virus infection in nonhuman primates. Sci Rep. 2020;10(1):13069.
761 26.   Han J, Wang B, Han N, Zhao Y, Song C, Feng X, et al. CD14(high)CD16(+) rather than
762 CD14(low)CD16(+) monocytes correlate with disease progression in chronic HIV-infected
763 patients. J Acquir Immune Defic Syndr. 2009;52(5):553-9.
764 27.   Chaplin JW, Chappell CP, Clark EA. Targeting antigens to CD180 rapidly induces
765 antigen-specific IgG, affinity maturation, and immunological memory. J Exp Med.
766 2013;210(10):2135-46.
767 28.   Erasmus JH, Khandhar AP, O'Connor MA, Walls AC, Hemann EA, Murapa P, et al. An
768 Alphavirus-derived replicon RNA vaccine induces SARS-CoV-2 neutralizing antibody and T cell
769 responses in mice and nonhuman primates. Sci Transl Med. 2020;12(555).
770 29.   Fennessey CM, Pinkevych M, Immonen TT, Reynaldi A, Venturi V, Nadella P, et al.
771 Genetically-barcoded SIV facilitates enumeration of rebound variants and estimation of
772 reactivation rates in nonhuman primates following interruption of suppressive antiretroviral
773 therapy. PLoS Pathog. 2017;13(5):e1006359.

774   30.   Tunggal HC, Munson PV, O'Connor MA, Hajari N, Dross SE, Bratt D, et al. Effects of
775   therapeutic vaccination on the control of SIV in rhesus macaques with variable responsiveness
776   to antiretroviral drugs. PLoS One. 2021;16(6):e0253265.
777   31.   Ho O, Larsen K, Polacino P, Li Y, Anderson D, Song R, et al. Pathogenic infection of
778   Macaca nemestrina with a CCR5-tropic subtype-C simian-human immunodeficiency virus.
779   Retrovirology. 2009;6:65.
780   32.   Davis MA, Voss K, Turnbull JB, Gustin AT, Knoll M, Muruato A, et al. A C57BL/6 Mouse
781   Model of SARS-CoV-2 Infection Recapitulates Age- and Sex-Based Differences in Human
782   COVID-19 Disease and Recovery. Vaccines (Basel). 2022;11(1).
783   33.   Tisoncik-Go J, Voss KM, Lewis TB, Muruato AE, Kuller L, Finn EE, et al. Evaluation of
784   the immunogenicity and efficacy of an rVSV vaccine against Zika virus infection in macaca
785   nemestrina. Front Virol. 2023;3.
786   34.   Richard AS, Shim BS, Kwon YC, Zhang R, Otsuka Y, Schmitt K, et al. AXL-dependent
787   infection of human fetal endothelial cells distinguishes Zika virus from other pathogenic
788   flaviviruses. Proc Natl Acad Sci U S A. 2017;114(8):2024-9.
789   35.   Liu S, DeLalio LJ, Isakson BE, Wang TT. AXL-Mediated Productive Infection of Human
790   Endothelial Cells by Zika Virus. Circ Res. 2016;119(11):1183-9.
791   36.   Meertens L, Labeau A, Dejarnac O, Cipriani S, Sinigaglia L, Bonnet-Madin L, et al. Axl
792   Mediates ZIKA Virus Entry in Human Glial Cells and Modulates Innate Immune Responses. Cell
793   Rep. 2017;18(2):324-33.
794   37.   Persaud M, Martinez-Lopez A, Buffone C, Porcelli SA, Diaz-Griffero F. Infection by Zika
795   viruses requires the transmembrane protein AXL, endocytosis and low pH. Virology.
796   2018;518:301-12.
797   38.   Wie SH, Du P, Luong TQ, Rought SE, Beliakova-Bethell N, Lozach J, et al. HIV
798   downregulates interferon-stimulated genes in primary macrophages. J Interferon Cytokine Res.
799   2013;33(2):90-5.
800   39.   Lu AY, Gustin A, Newhouse D, Gale M, Jr. Viral Protein Accumulation of Zika Virus
801   Variants Links with Regulation of Innate Immunity for Differential Control of Viral Replication,
802   Spread, and Response to Interferon. J Virol. 2023;97(5):e0198222.
803   40.   Esser-Nobis K, Aarreberg LD, Roby JA, Fairgrieve MR, Green R, Gale M, Jr.
804   Comparative Analysis of African and Asian Lineage-Derived Zika Virus Strains Reveals
805   Differences in Activation of and Sensitivity to Antiviral Innate Immunity. J Virol. 2019;93(13).
806   41.   Berry N, Kempster S, Ham C, Jenkins A, Hall J, Page M, et al. Passive immunisation of
807   convalescent human anti-Zika plasma protects against challenge with New World Zika virus in
808   cynomolgus macaques. NPJ Vaccines. 2020;5:86.
809   42.   McDonald EM, Anderson J, Wilusz J, Ebel GD, Brault AC. Zika Virus Replication in
810   Myeloid Cells during Acute Infection Is Vital to Viral Dissemination and Pathogenesis in a
811   Mouse Model. J Virol. 2020;94(21).
812   43.   de Siqueira Santos R, Rochael NC, Mattos TRF, Fallett ESMF, Linhares-Lacerda L, de
813   Oliveira LT, et al. Peripheral nervous system is injured by neutrophil extracellular traps (NETs)
814   elicited by nonstructural (NS) protein-1 from Zika virus. Faseb j. 2023;37(9):e23126.
815   44.   Siong WC, Ching TH, Jong GC, Pang CS, Vernon LJ, Sin LY. Dengue infections in HIV
816   patients. Southeast Asian J Trop Med Public Health. 2008;39(2):260-5.
817   45.   Torrentes-Carvalho A, Hottz ED, Marinho CF, da Silva JB, Pinto LM, Fialho LG, et al.
818   Characterization of clinical and immunological features in patients coinfected with dengue virus
819   and HIV. Clin Immunol. 2016;164:95-105.
820   46.   Delgado-Enciso I, Espinoza-Gómez F, Ochoa-Jiménez R, Valle-Reyes S, Vásquez C,
821   López-Lemus UA. Dengue Infection in a Human Immunodeficiency Virus-1 Positive Patient
822   Chronically Infected with Hepatitis B Virus in Western Mexico. Am J Trop Med Hyg.
823   2017;96(1):122-5.

824 47.   Joao EC, Ferreira ODC, Jr., Gouvea MI, Teixeira MLB, Tanuri A, Higa LM, et al.
825 Pregnant women co-infected with HIV and Zika: Outcomes and birth defects in infants according
826 to maternal symptomatology. PLoS One. 2018;13(7):e0200168.
827 48.   Shapiro-Mendoza CK, Rice ME, Galang RR, Fulton AC, VanMaldeghem K, Prado MV,
828 et al. Pregnancy Outcomes After Maternal Zika Virus Infection During Pregnancy - U.S.
829 Territories, January 1, 2016-April 25, 2017. MMWR Morb Mortal Wkly Rep. 2017;66(23):615-21.
830 49.   Rosinski JR, Raasch LE, Barros Tiburcio P, Breitbach ME, Shepherd PM, Yamamoto K,
831 et al. Frequent first-trimester pregnancy loss in rhesus macaques infected with African-lineage
832 Zika virus. PLoS Pathog. 2023;19(3):e1011282.
833 50.   Vinton CL, Magaziner SJ, Dowd KA, Robertson SJ, Amaro-Carambot E, Karmele EP, et
834 al. Simian Immunodeficiency Virus Infection of Rhesus Macaques Results in Delayed Zika Virus
835 Clearance. mBio. 2019;10(6).
836 51.   Bidokhti MRM, Dutta D, Madduri LSV, Woollard SM, Norgren R, Jr., Giavedoni L, et al.
837 SIV/SHIV-Zika co-infection does not alter disease pathogenesis in adult non-pregnant rhesus
838 macaque model. PLoS Negl Trop Dis. 2018;12(10):e0006811.
839 52.   Debiasi RL, Tyler KL. West Nile virus meningoencephalitis. Nat Clin Pract Neurol.
840 2006;2(5):264-75.
841 53.   Parra B, Lizarazo J, Jiménez-Arango JA, Zea-Vera AF, González-Manrique G, Vargas J,
842 et al. Guillain-Barré Syndrome Associated with Zika Virus Infection in Colombia. N Engl J Med.
843 2016;375(16):1513-23.
844 54.   Aid M, Abbink P, Larocca RA, Boyd M, Nityanandam R, Nanayakkara O, et al. Zika Virus
845 Persistence in the Central Nervous System and Lymph Nodes of Rhesus Monkeys. Cell.
846 2017;169(4):610-20.e14.
847 55.   Coffey LL, Pesavento PA, Keesler RI, Singapuri A, Watanabe J, Watanabe R, et al. Zika
848 Virus Tissue and Blood Compartmentalization in Acute Infection of Rhesus Macaques. PLoS
849 One. 2017;12(1):e0171148.
850 56.   Hirsch AJ, Smith JL, Haese NN, Broeckel RM, Parkins CJ, Kreklywich C, et al. Zika
851 Virus infection of rhesus macaques leads to viral persistence in multiple tissues. PLoS Pathog.
852 2017;13(3):e1006219.
853 57.   Hsu DC, Chumpolkulwong K, Corley MJ, Hunsawong T, Inthawong D, Schuetz A, et al.
854 Neurocognitive impact of Zika virus infection in adult rhesus macaques. J Neuroinflammation.
855 2022;19(1):40.
856 58.   Panganiban AT, Blair RV, Hattler JB, Bohannon DG, Bonaldo MC, Schouest B, et al. A
857 Zika virus primary isolate induces neuroinflammation, compromises the blood-brain barrier and
858 upregulates CXCL12 in adult macaques. Brain Pathol. 2020;30(6):1017-27.
859 59.   Miller CJ, Manuzak JA, Gustin AT, Basting CM, Cheu RK, Schroeder TA, et al. Elevated
860 peripheral and nervous system inflammation is associated with decreased short-chain fatty acid
861 levels in Zika-virus infected macaques. bioRxiv. 2023:2023.07.25.550459.
862 60.   Jamison SC, Michaels SR, Ratard R, Sweet JM, Deboisblanc BP. A 41-year-old HIV-
863 positive man with acute onset of quadriplegia after West Nile virus infection. South Med J.
864 2007;100(10):1051-3.
865 61.   Josekutty J, Yeh R, Mathew S, Ene A, Ramessar N, Trinidad J. Atypical presentation of
866 West Nile virus in a newly diagnosed human immunodeficiency virus patient in New York City. J
867 Clin Microbiol. 2013;51(4):1307-9.
868 62.   Torno M, Vollmer M, Beck CK. West Nile virus infection presenting as acute flaccid
869 paralysis in an HIV-infected patient: a case report and review of the literature. Neurology.
870 2007;68(7):E5-7.
871 63.   Wang Y, Ling L, Zhang Z, Marin-Lopez A. Current Advances in Zika Vaccine
872 Development. Vaccines (Basel). 2022;10(11).

873 64.   Schouest B, Beddingfield BJ, Gilbert MH, Bohm RP, Schiro F, Aye PP, et al. Zika virus
874 infection during pregnancy protects against secondary infection in the absence of CD8(+) cells.
875 Virology. 2021;559:100-10.
876 65.   Marzan-Rivera N, Serrano-Collazo C, Cruz L, Pantoja P, Ortiz-Rosa A, Arana T, et al.
877 Infection order outweighs the role of CD4(+) T cells in tertiary flavivirus exposure. iScience.
878 2022;25(8):104764.
879 66.   Proal AD, VanElzakker MB, Aleman S, Bach K, Boribong BP, Buggert M, et al. SARS-
880 CoV-2 reservoir in post-acute sequelae of COVID-19 (PASC). Nat Immunol. 2023;24(10):1616-
881 27.
882 67.   Yendewa GA, Perez JA, Patil N, McComsey GA. Associations between post-acute
883 sequelae of SARS-CoV-2, COVID-19 vaccination and HIV infection: a United States cohort
884 study. Front Immunol. 2024;15:1297195.
885

886 **Supporting information captions**

887 *Supporting Information File 1*. Animal characteristics, SIV plasma load, and peripheral CD4

888 counts

889 *Supporting Information File 2*. Gross and histopathologic assessment

890 *Supporting Information File 3*. Primary antibodies used for immunophenotyping analysis

891 *Supporting Information File 4*. Post-SIV PBMC gene expression for genes shown in **Figure 1D**

892 *Supporting Information File 5*. Post-ZIKV PBMC gene expression for genes shown in **Figure 5A**

893 *Supporting Information File 6*. PBMC gene expression kinetics for SIV+ZIKV+ and SIV-ZIKV+

894 groups shown in **Figure 5C**

895 *Supporting Information File 7*. ZIKV RNA quantitation in longitudinal samples

896 *Supporting Information File 8*. ZIKV RNA quantitation in necropsy samples
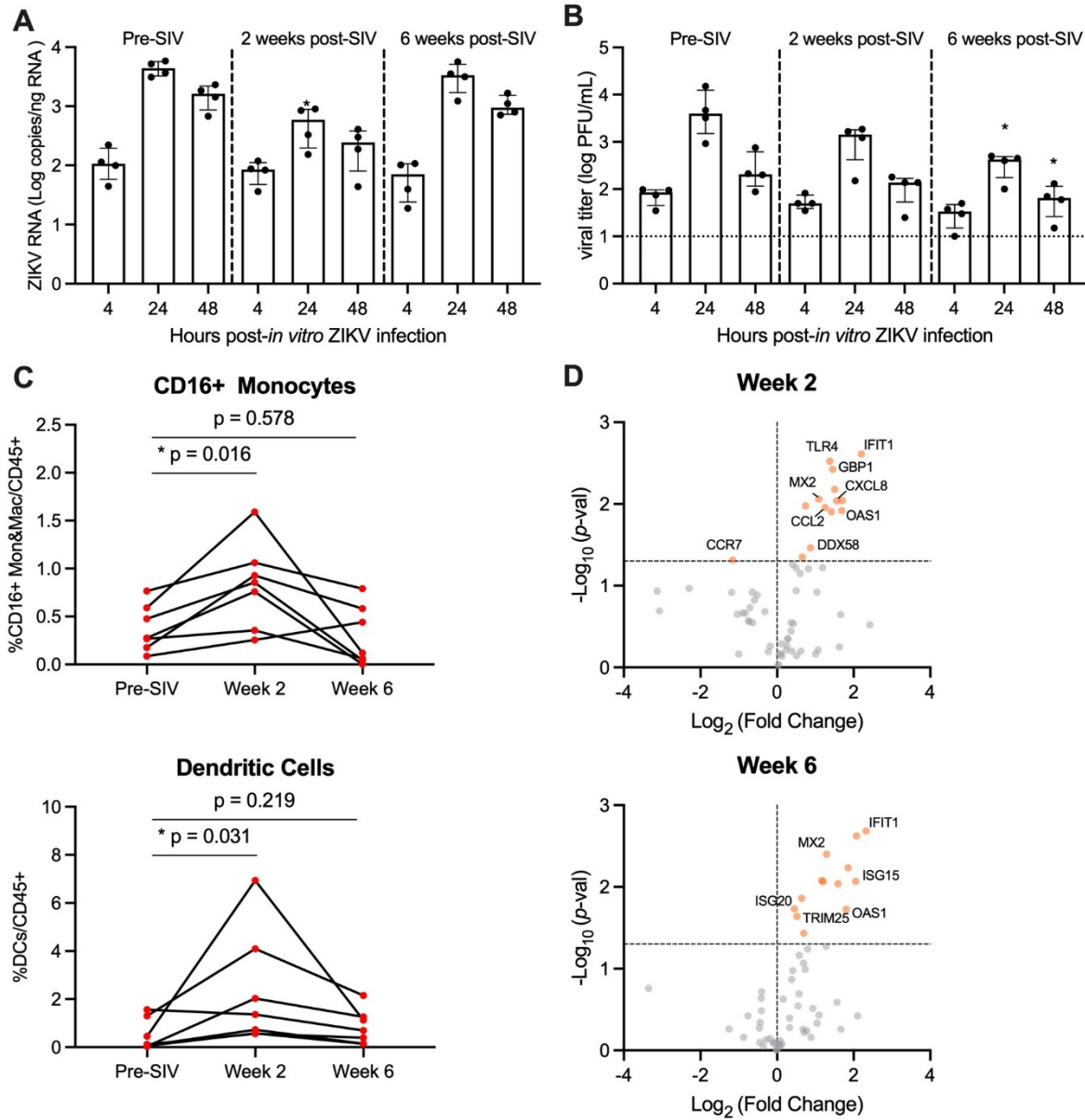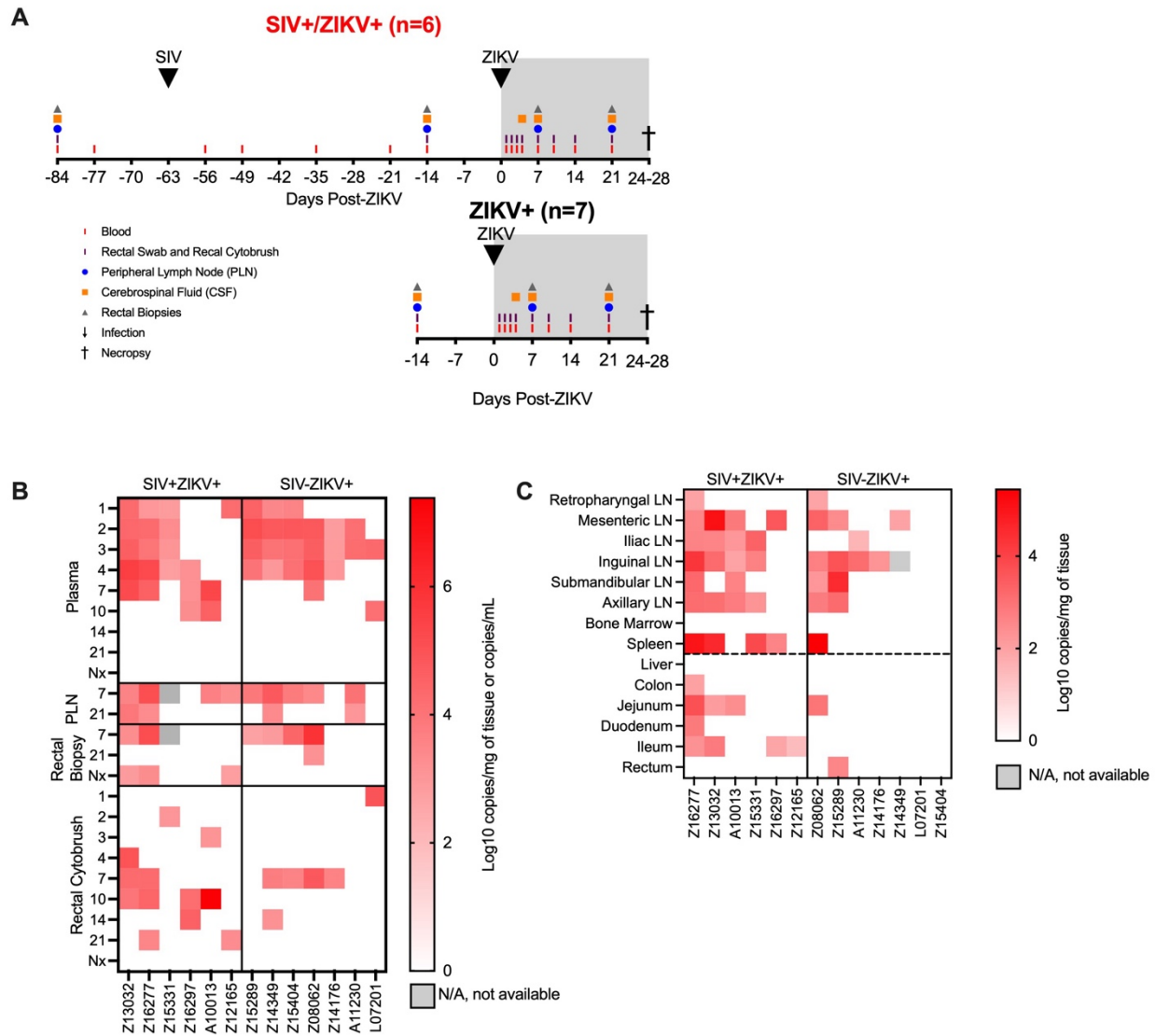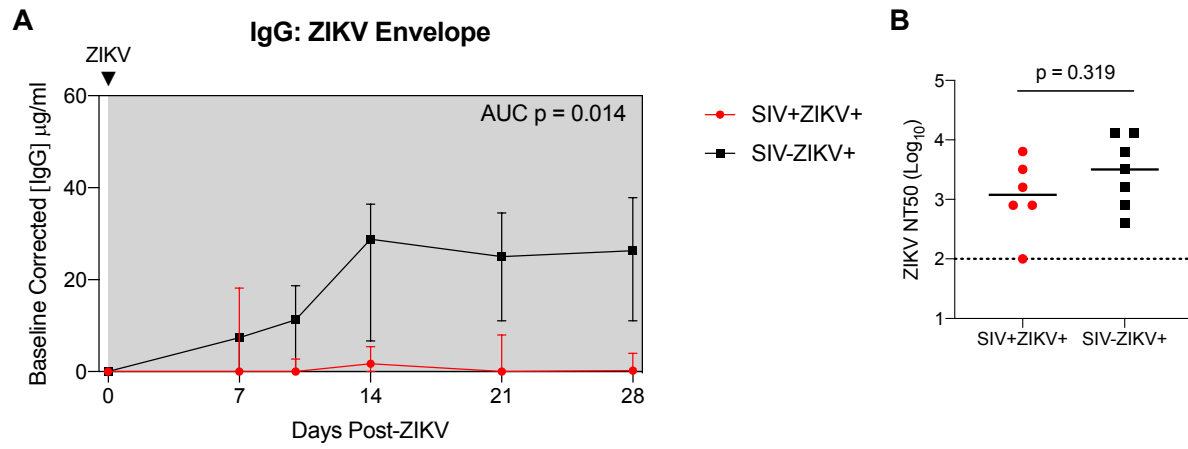
897

Figure 1.
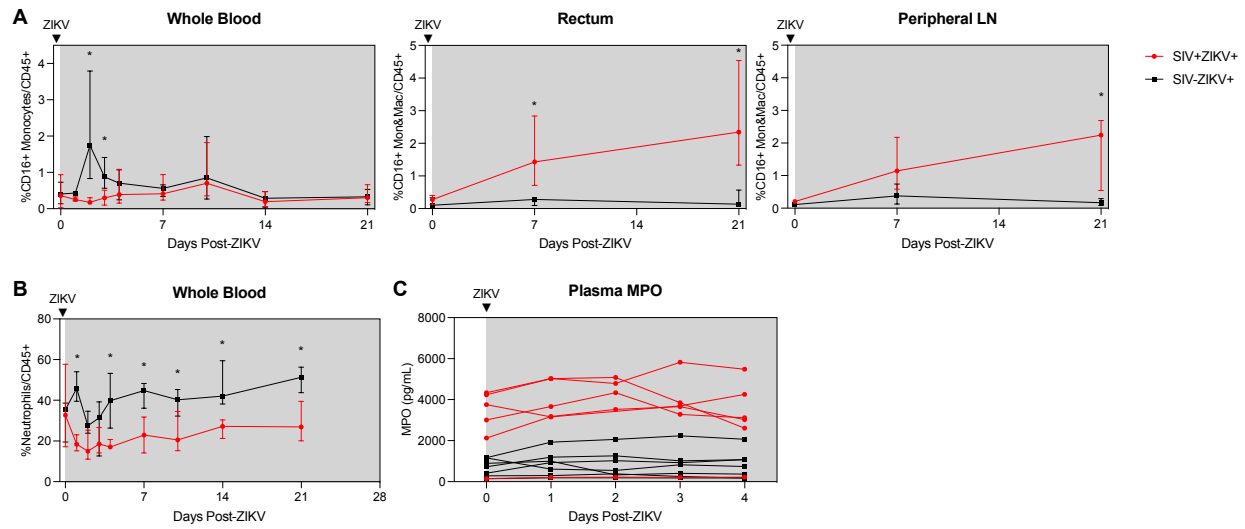
Figure 2.

Figure 3.

A — IgG: ZIKV Envelope

AUC p = 0.014

- SIV+ZIKV+
- SIV-ZIKV+

B

p = 0.319

Figure 4.

Figure 5.

Figure 6.